

Allosteric impurity effects in long spin chains

Christian Eidecker-Dunkel and Peter Reimann

Faculty of Physics, Bielefeld University, 33615 Bielefeld, Germany

(Dated: August 11, 2023)

Allosterism traditionally refers to local changes in an extended object, for instance the binding of a ligand to a macromolecule, leading to a localized response at some other, possibly quite remote position. Here, we show that such fascinating effects may already occur in very simple and common quantum many-body systems, such as an anisotropic Heisenberg spin chain: Introducing an impurity at one end of a sufficiently long chain may lead to quite significant changes of the observable behavior near the other end, but not in the much larger region in between. Specifically, spin autocorrelation functions at thermal equilibrium are found to exhibit a pronounced allosterism of this type.

I. INTRODUCTION

It is commonly taken for granted that isolated many-body systems with short-range interactions satisfy a locality principle of the following kind: A single defect, impurity, or other type of local modification does not lead to significant changes of the systems' thermal equilibrium properties at sufficiently remote places. The main message of our present work consists in the discovery that exactly the opposite behavior actually occurs already for very simple examples such as an anisotropic Heisenberg spin chain: Thermal equilibrium correlation functions near *both* ends of the chain may exhibit quite substantial changes upon introducing an impurity at one end. Moreover, no significant changes of the thermal equilibrium properties are observed throughout the rest of the chain. Since such a phenomenon is somewhat reminiscent of the “action at a distance” effects in the context of allosteric biochemical processes, we will adopt here the same label of “allosterism” to our present case.

Closely related systems, but with the impurity being located in the middle of a spin chain with open boundary conditions, have been recently explored quite extensively for example in Refs. [1–5]. The main focus in these works is on the (non-)integrability, relaxation, and transport properties of models which, in the absence of the impurity, are integrable, and therefore do not approach thermal equilibrium after a quantum quench [6–13]. Remarkably, when switching on the impurity, those systems were numerically found in Refs. [1–5] to become non-integrable and thus to exhibit thermalization after a quench. More precisely speaking, upon parametrically changing the impurity strength, a continuous transition was numerically observed, which becomes more and more rapid as the chain length is increased, implying that in the thermodynamic limit an arbitrarily weak impurity would be sufficient to instantly turn a non-thermalizing system into a thermalizing one [4] (see also [2, 3]).

It is well-known, yet quite remarkable in view of these integrability-breaking effects of a *mid-chain* impurity, that the same type of impurity at the *end* of the chain provably preserves the system's integrability [14–16]. Here, we will show that even more remarkable effects, namely allosterism, may be caused by such an end-

impurity.

An important difference compared to the previous Refs. [1–5] is that we focus on systems which are at thermal equilibrium from the outset. On the other hand, our findings are – similar to those in Refs. [1–5] – mainly based on numerical explorations, complemented by some analytical insights.

II. SETTING

We consider the familiar anisotropic spin-1/2 Heisenberg chain (XYZ model), exhibiting open boundary conditions and a magnetic impurity at the “left end”,

$$H = g s_1^z - \sum_{l=1}^{L-1} J_x s_{l+1}^x s_l^x + J_y s_{l+1}^y s_l^y + J_z s_{l+1}^z s_l^z, \quad (1)$$

where $s_l^{x,y,z}$ are spin-1/2 operators at the lattice sites $l \in \{1, \dots, L\}$ (lattice constant one), and g quantifies the strength of the impurity.

We mostly restrict ourselves to even L and pairwise different $J_{x,y,z}$ (generalizations will be briefly addressed in Sec. S4). The reason is that under these conditions we numerically observed that all the subsequently explored Hamiltonians (1) did not exhibit any degeneracies, which in turn allows us to make some interesting analytical predictions. Hereafter, we just state those predictions whenever appropriate, referring to the accompanying Supplemental Material [17] for their detailed derivation. We also prove in [17] that H necessarily must exhibit degeneracies for $g = 0$ if L is odd or the $J_{x,y,z}$ are not pairwise different, hence some of our analytical predictions no longer apply.

As announced, the system is assumed to be at thermal equilibrium, described by a canonical ensemble $e^{-\beta H} / \text{tr}\{e^{-\beta H}\}$ with temperature β^{-1} (Boltzmann constant $k_B = 1$). Accordingly, thermal expectation values of an observable A are given by

$$\langle A \rangle_{\text{th}} := \text{tr}\{A e^{-\beta H}\} / \text{tr}\{e^{-\beta H}\} \quad (2)$$

and dynamic (auto-)correlation functions by

$$C_t(A) := \langle AA(t) \rangle_{\text{th}} - \langle A \rangle_{\text{th}}^2, \quad (3)$$

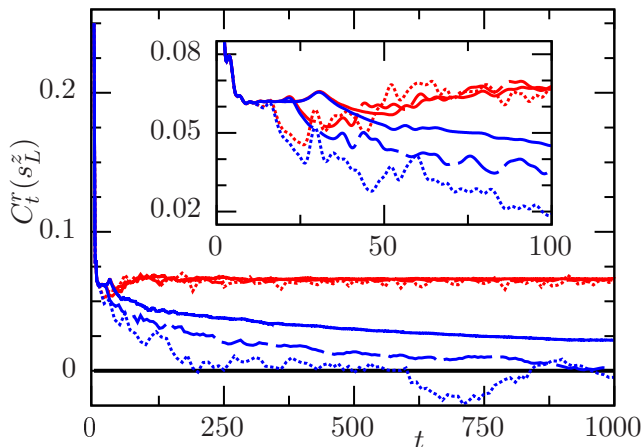


FIG. 1. Numerically obtained correlation functions $C_t^r(s_L^z)$ from (4) versus time [18]. Red: XYZ model (1) with $g = 0.1$, $L = 20$ (solid), $L = 14$ (dashed), $L = 10$ (dotted), $J_x = 1$, $J_y = 1.2$, $J_z = 1.5$, and $\beta = 0.2$. Blue: Same, but for $g = 0$. Inset: Magnification for $t \leq 100$.

where $A(t) := e^{iHt} A e^{-iHt}$ (Heisenberg picture, $\hbar = 1$). Furthermore, their real (or symmetrized) part

$$C_t^r(A) := \text{Re}\{C_t(A)\} \quad (4)$$

is usually of major interest (see also discussion below Eq. (7)).

III. RESULTS

Figure 1 exemplifies the correlations (4) of the magnetization $A = s_L^z$ at the chain's “right end” ($l = L$). The salient point is that these correlations exhibit significant differences depending on whether an impurity at the opposite end ($l = 1$) is present ($g \neq 0$, red curves) or not ($g = 0$, blue curves). The differences become clearly visible for $t \gtrsim 1.5L$ (see inset), while all curves nearly coincide for $t \lesssim 1.5L$. Intuitively, this may be understood as the signature of a maximal speed at which information about the situation at one end can travel to the other end [19–23]. Likewise, one may understand why the growth of those differences slows down when L increases [24]. Yet, they ultimately always approach a sizable, and asymptotically L -independent long-time limit (see also the subsequent paragraphs), i.e., an impurity at one end quite notably affects the correlation functions at the other end.

Similarly as in Fig. 1, we numerically explored the correlation functions for various other observables, most notably or s_l^a with $a \in \{x, y, z\}$ and $l \in \{1, \dots, L\}$. Again, we found that if some non-negligible difference in the absence ($g = 0$) and in the presence ($g \neq 0$) of the impurity was observable at all, then this difference predominantly manifested itself after sufficiently long times. Henceforth, we thus restrict ourselves to the long-time behavior of the

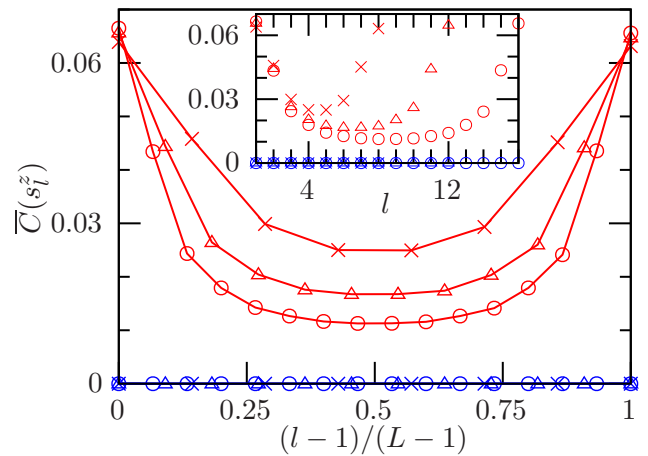


FIG. 2. Long-time average $\overline{C}(s_l^z)$ from (7) versus chain site $l = 1, \dots, L$ [18]. Red: XYZ model (1) with $g = 0.1$, $L = 16$ (circles), $L = 12$ (triangles), $L = 8$ (stars), $J_x = 1$, $J_y = 1.2$, $J_z = 1.5$, and $\beta = 0.2$. Blue: Same, but for $g = 0$. Inset: Raw data. Main plot: Rescaled x -axis and interpolating lines to guide the eye.

correlations $C_t(A)$, in particular their long-time average

$$\overline{C}(A) := \lim_{T \rightarrow \infty} \frac{1}{T} \int_0^T dt C_t(A). \quad (5)$$

Indeed, one intuitively expects that, after initial transients have died out, the time-dependent correlations $C_t(A)$ stay closer and closer to the time-averaged value $\overline{C}(A)$ as the system size L increases. A typical example is provided by the red curves in Fig. 1, and further examples can be seen in Figs. S3 and S4 of the Supplemental Material [17]. We also observed this expected long-time behavior in all other numerical examples which we explored with respect to these specific features. The same has even been shown analytically under very weak assumptions regarding the spectrum of H in Ref. [25] (see also [26]). Accordingly, we henceforth take it for granted that $\overline{C}(A)$ faithfully captures the long-time behavior of $C_t(A)$.

Denoting by E_n and $|n\rangle$ the eigenvalues and eigenvectors of the Hamiltonian H (with $n = 1, \dots, N := 2^L$), one readily infers [25, 27] from (2), (3), and (5) that

$$\langle A \rangle_{\text{th}} = \sum_{n=1}^N p_n \langle n|A|n \rangle, \quad (6)$$

$$\overline{C}(A) = \sum_{n=1}^N p_n [\langle n|A|n \rangle - \langle A \rangle_{\text{th}}]^2, \quad (7)$$

where $p_n := e^{-\beta E_n} / \sum_{m=1}^N e^{-\beta E_m}$ is the population of the energy level $|n\rangle$ in the canonical ensemble, and where – in case that H exhibits degeneracies – the eigenstates $|n\rangle$ must be chosen so that A is diagonal in the corresponding eigenspaces of H (see also the Supplemental Material [17]). As an aside, we can infer from (7) that the

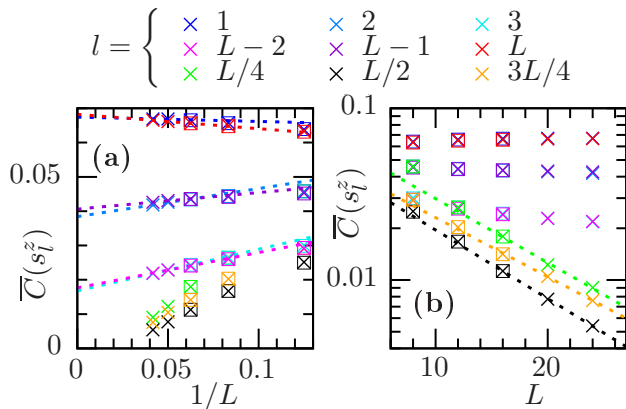


FIG. 3. (a) Long-time average $\overline{C}(s_l^z)$ versus $1/L$ for various l -values (see legend), employing the same model as in Fig. 2 ($g = 0.1$). Crosses: Numerical results by evaluating (5) for large but finite T [18]. Squares: Numerically exact (but also more expensive) results by evaluating (7) via diagonalization of H . Some symbols are (nearly) covered by others. (b) Same data, but plotted semi-logarithmically versus L . The dotted lines are a guide to the eye, suggesting for the corresponding l -values a convergence towards a positive large- L limit in (a) and an exponential decay towards zero in (b), see also main text.

long-time average in (5) must be real and non-negative. Moreover, it must be equal to the long-time average of the real part $C_l^r(A)$ from (4).

Assuming $g = 0$ (no impurity), and exploiting that H exhibits no degeneracies (see below Eq. (1)), we analytically show in [17] that $\langle n|s_l^a|n \rangle = 0$ for all n, l , and $a \in \{x, y, z\}$. Hence, the thermal expectation values in (6) as well as the long-time averages in (7) must vanish for all $A = s_l^a$. In particular,

$$\langle s_L^z \rangle_{\text{th}} = 0 \text{ and } \overline{C}(s_L^z) = 0 \text{ if } g = 0, \quad (8)$$

i.e., all the blue curves in Fig. 1 must end up by fluctuating around zero. If $g \neq 0$, we furthermore prove in [17] that thermal expectation values and long-time averages still vanish for all $A = s_l^{x,y}$, while $A = s_l^z$ must now be evaluated numerically.

Figure 2 shows such numerically obtained long-time averages for $A = s_l^z$, implying: (i) As analytically predicted, $\overline{C}(s_l^z) = 0$ for $g = 0$ (blue symbols). (ii) Upon increasing L , the impurity effects (difference between blue and red symbols) decrease outside the two end regions, while they even slightly increase at the two ends. (iii) The values of $\overline{C}(s_l^z)$ and $\overline{C}(s_{L+1-l}^z)$ are nearly equal for $g = 0.1$ (red symbols).

Concerning (ii), a more detailed finite-size scaling analysis is presented in Fig. 3. Our first remark is that crosses and squares have been obtained by means of two entirely different numerical methods. Their close agreement indicates that our numerics is trustworthy. We also note that the crosses were numerically less expensive, hence larger L values could be achieved. Furthermore, the dotted lines in Fig. 3(a) indicate that $\overline{C}(s_l^z)$

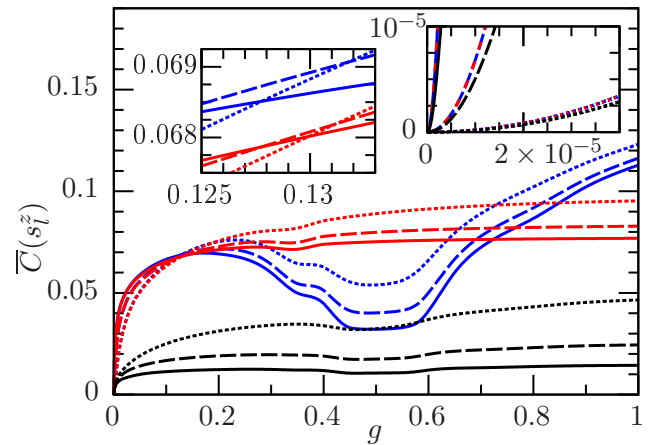


FIG. 4. Long-time average $\overline{C}(s_l^z)$ from (7) versus impurity strength g [18] for $l = 1$ (blue), $l = L$ (red), $l = L/2$ (black), $L = 16$ (solid), $L = 12$ (dashed), $L = 8$ (dotted), $J_x = 1$, $J_y = 1.2$, $J_z = 1.5$, and $\beta = 0.2$. Insets: Magnifications near $g = 0.13$ (left) and $g = 0$ (right).

converges, for an arbitrary but fixed $l \in \{1, 2, 3\}$, towards a non-vanishing limit when $L \rightarrow \infty$, and likewise when keeping $L - l \in \{0, 1, 2\}$ fixed. While these limiting values clearly decrease with increasing $l \in \{1, 2, 3\}$ or $L - l \in \{0, 1, 2\}$, it nevertheless seems reasonable to expect that $\overline{C}(s_l^z)$ still asymptotically approaches some non-vanishing limit whenever l or $L - l$ is kept at an arbitrary but fixed value as $L \rightarrow \infty$. Indeed, the alternative option that the limit stays finite up to some maximal distance from the chain ends, and then strictly vanishes, appears less reasonable. On the other hand, for an arbitrary but fixed $l/L \in \{1/4, 1/2, 3/4\}$ the numerical data in Fig. 3(a) apparently approach zero faster than $1/L$, while the dotted lines in Fig. 3(b) indicate that they asymptotically decrease exponentially with L . Again, it thus seems reasonable to expect such an exponential decay whenever l/L converges to a limit different from zero and unity. Additional data in support of these predictions are provided in [17].

Altogether, we thus recover the announced allosteric impurity effects for long spin chains, complemented by rather interesting finite-size scaling properties.

Next we turn to the dependence of the long-time correlations $\overline{C}(s_l^z)$ on the impurity strength g . Focusing on the ends and the center of the chain, i.e., on $l \in \{1, L/2, L\}$, a numerical example is depicted in Fig. 4. Furthermore, a finite-size scaling analysis analogous to that in Fig. 3(a) is provided in Fig. 5 for a few representative g -values. The corresponding counterpart of Fig. 3(b) is available as Supplemental Material [17]. Similarly as before, these numerical findings indicate that $\overline{C}(s_l^z)$ converges to a non-vanishing limit for $l = 1$ and $l = L$, and decays to zero for $l = L/2$. Furthermore, it seems again reasonable to expect that the same qualitative large- L asymptotics will apply to any given $g > 0$, and likewise for other l -values (see above).

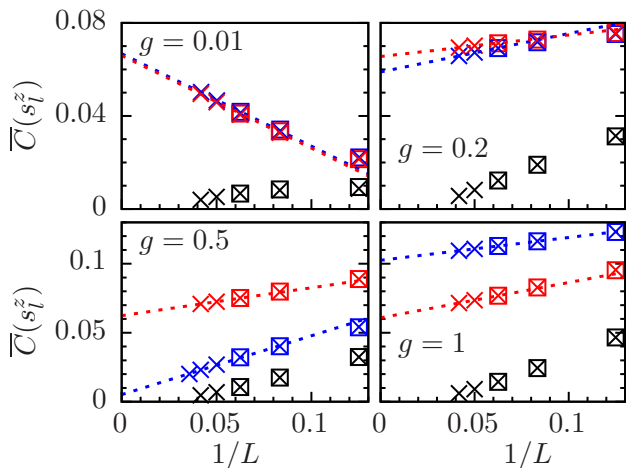


FIG. 5. Same as in Fig. 3(a) for $l = 1$ (blue), $l = L$ (red), $l = L/2$ (black), but now for different coupling strengths g (see legends). For $g = 0.5$, an extremely expensive extra blue cross at $L = 28$ has been generated in support of a non-vanishing large- L limit.

Regarding the issue (iii) from above (see paragraph below Eq. (8)), Figs. 3-5 confirm that $\bar{C}(s_l^z)$ and $\bar{C}(s_{L+1-l}^z)$ are indeed nearly indistinguishable if (and only if) g is sufficiently small. Further interesting features of Fig. 4 are the local minima near $g = 1/2$ (blue and black) and $g = 1/3$ (red), and the closeness of the crossing points near $g = 0.13$ (left inset). Additional details are deferred to the Supplemental Material [17] since all these “extra features” go beyond our actual main objective, namely to demonstrate the occurrence of allosteric impurity effects *per se*.

As already mentioned, for $g = 0$ we analytically established in [17] that $\bar{C}(s_l^z) = 0$. Yet another analytical prediction in [17] is the invariance of $\bar{C}(s_l^z)$ under a sign change of g . This justifies our restriction to $g \geq 0$ in the numerics, and suggests that $\bar{C}(s_l^z) \sim g^2$ for asymptotically small g . The right inset of Fig. 4 confirms this quadratic asymptotics, and indicates that the curvature $\partial^2 \bar{C}(s_l^z) / \partial g^2 |_{g=0}$ actually diverges as $L \rightarrow \infty$. Overall, the behavior for $g \rightarrow 0$ and $L \rightarrow \infty$ is thus quite intriguing, and in fact somewhat reminiscent of the integrability-breaking effects of an impurity in the middle of the chain (see second paragraph in Sec. S1).

IV. GENERALIZATIONS AND DISCUSSION

Our findings for more general model parameters are summarized in the following items (a) to (e), postponing their detailed analytical and numerical substantiation to the accompanying Supplemental Material [17]: (a) If L is odd or the $J_{x,y,z}$ are not pairwise different (see below Eq. (1)), then our analytical result $\bar{C}(s_l^z) = 0$ for $g = 0$ is no longer valid. Accordingly, the behavior of $\bar{C}(s_l^z)$ for $g = 0$, henceforth abbreviated as $\bar{C}_0(s_l^z)$, must be numer-

ically explored, and the characteristic signatures of allostery are now captured by $\Delta \bar{C}(s_l^z) := \bar{C}(s_l^z) - \bar{C}_0(s_l^z)$. We numerically found that $\Delta \bar{C}(s_l^z)$ still behaves qualitatively similarly as in Figs. 2-5, i.e., the system again exhibits the same allosteric impurity effects as before. (b) We also observed a qualitatively similar behavior for various other β -values in (2). (c) The same applies to other values of $J_{x,y,z}$ in (1) at least within the realm $J_z > J_{x,y} \geq 0$ (and excepting $J_x = J_y = 0$). Quite surprisingly, however, the allosteric effects are found to disappear when $J_x \geq J_{y,z} \geq 0$ or $J_y \geq J_{x,z} \geq 0$. (d) It is sufficient to focus on non-negative interactions $J_{x,y,z}$ in Eq. (1) since the behavior in all other cases can be inferred by symmetry arguments. (e) Instead of the canonical ensemble in Eq. (2), one may as well employ a microcanonical ensemble, i.e., our allosteric effects exhibit the usual equivalence of ensemble properties [28].

Figure 4 and its discussion, as well as the above mentioned observation (c) indicate that figuring out the basic physical mechanism behind our allosteric effects represents a very challenging task. This is further corroborated by the following two remarks: (i) As far as “ordinary” thermal expectation values (2) are concerned, we never found any noteworthy impact of the impurity on the system’s equilibrium properties sufficiently far away from that impurity. In particular, for the observable $A = s_L^z$ we thus can conclude with (8) that $\langle s_L^z \rangle_{\text{th}} = 0$ is still fulfilled in very good approximation even if $g \neq 0$, and provided L is sufficiently large. In other words, our present allosteric effects only manifest themselves in the correlation functions from (3), not in the expectation values from (2), the key signature being a non-vanishing thermodynamic limit of $\bar{C}(s_l^z)$ for $g \neq 0$. (ii) Generally speaking, such a non-vanishing thermodynamic limit of $\bar{C}(A)$ is already in itself a quite exceptional situation [29]. The only previous examples known to us are a few, rather special spin-chain and central spin models, see Refs. [24, 27, 30–33] and further references therein. Most notably, XX-chains with open boundary conditions and local impurities of a different type than in (1) have been numerically and analytically explored in Ref. [31], explaining some of the therein observed impurity effects in terms of localized single-particle “boundary modes” after mapping the model by means of a Jordan-Wigner transformation to a formally equivalent system of non-interacting fermions. However, we found that our present allostery does *not* occur in those XX-chain models from [31] (see also item (c) above), and that the analytical methods from [27, 30, 31] cannot be adapted to explain our present allosteric effects. In particular, the boundary modes from Ref. [31] become meaningless since our present Hamiltonians (1) can no longer be mapped to a model of non-interacting fermions. We also remark that a similar observation as in (c) above has been previously reported in Sec. 2.4 of Ref. [30] for an XY-model in the infinite temperature limit, and most importantly, *without* any impurity [34].

On the other hand, many essential features of the blue

curves in Fig. 1 can be analytically understood [24] by means of so-called edge zero modes [35]. In particular, these insights are in agreement with our numerical observation that the blue and red curves in Fig. 1 nearly coincide for $t \lesssim 1.5L$. Focusing on the thermodynamic limit $L \rightarrow \infty$ is therefore useless for the exploration of our present allosteric effects, as done, for instance, in the analytical investigations in Refs. [33, 36] of certain impurity effects in the XXZ model.

Incidentally, taking for granted the so-called eigenstate thermalization hypothesis (ETH) [9] and the usual equivalence of ensembles [28], one can conclude that the long-time average in Eq. (7) must asymptotically vanish for large L , and that our present allosteric effects can thus be ruled out. In fact, the same conclusion can already be deduced [25] from a considerably weaker version of this standard ETH [9]. While the standard ETH is a still unproven conjecture concerning non-integrable models, this weaker version of the ETH is provably fulfilled by a very large class of translationally invariant models (integrable or not) with short-range interactions [37]. Overall, an indispensable (but not sufficient) prerequisite for the appearance of our present allosteric effects thus seems to be a violation of both the standard and the weak versions of the ETH, which in turn require that the system must be integrable [9] and not translationally invariant [25, 37], respectively.

Altogether, it seems reasonable to suspect that our allosteric impurity effects might be somehow related to the above mentioned concepts of boundary or edge zero modes, and to the (weak) ETH, but we are not aware of any previously established analytical tools or intuitive arguments which would admit some seizable further progress along these lines.

V. CONCLUSIONS

Our main result consists in the discovery of allosteric impurity effects in long spin chains. These effects seem to us quite remarkable in themselves, and comparable find-

ings in such relatively simple many-body systems with short-range interactions have to our knowledge never been observed before. A very interesting next step will be to explore the behavior in response to time-dependent changes of the end-impurity strength g in Eq. (1). In the not unlikely case that a notable response will again be detectable at the other chain end, but not outside the two end regions (for sufficiently long chains), this may open up a conceptually new way of secure quantum communication.

Superficially, our present allosteric effects might seem to be at least conceptually somehow related to the celebrated non-locality property of quantum mechanics (Einstein-Podolsky-Rosen paradox), or to the so-called cluster decomposition principle [38], but a closer look reveals that both of them are in fact not very helpful for a better understanding of our present case [41]. Likewise, our findings are somewhat reminiscent of allosteric biochemical processes, while the underlying physical mechanism and the way in which the effect actually manifests itself are clearly very different.

Another main message of our paper is that the occurrence (or not), as well as the quantitative details of our allosteric effects depends in a very subtle manner on the various model parameters. For instance, the relative magnitude of the three interactions $J_{x,y,z}$ in Eq. (1) seems to play a decisive role. Accordingly, an analytical or intuitive explanation of our numerical observations amounts to a quite challenging open problem for future studies.

ACKNOWLEDGMENTS

This work was supported by the Deutsche Forschungsgemeinschaft (DFG, German Research Foundation) within the Research Unit FOR 2692 under Grant No. 355031190, and by the Paderborn Center for Parallel Computing (PC²) within the project HPC-PRF-UBI2.

-
- [1] L. F. Santos, Integrability of a disordered Heisenberg spin-1/2 chain, *J. Phys. A* **37**, 4723 (2004).
 - [2] E. J. Torres-Herrera and L. F. Santos, Local quenches with global effects in interacting quantum systems, *Phys. Rev. E* **89**, 062110 (2014).
 - [3] L. F. Santos, F. Pérez-Bernal, and E. J. Torres-Herrera, Speck of chaos, *Phys. Rev. Research* **2**, 043034 (2020).
 - [4] M. Pandey, P. W. Claeys, D. K. Campbell, A. Polkovnikov, and D. Sels, Adiabatic eigenstate deformations as a sensitive probe for quantum chaos, *Phys. Rev. X* **10**, 041017 (2020).
 - [5] M. Brenes, T. LeBlond, J. Goold, and M. Rigol, Eigenstate Thermalization in a Locally Perturbed Integrable System, *Phys. Rev. Lett.* **125**, 070605 (2020).
 - [6] M. Ueda, Quantum equilibration, thermalization and prethermalization in ultracold atoms, *Nat. Rev. Phys.* **2**, 669 (2020).
 - [7] T. Mori, T. N. Ikeda, E. Kaminishi, and M. Ueda, Thermalization and prethermalization in isolated quantum systems: a theoretical overview, *J. Phys. B* **51**, 112001 (2018).
 - [8] C. Gogolin and J. Eisert, Equilibration, thermalization, and the emergence of statistical mechanics in closed quantum systems, *Rep. Prog. Phys.* **79**, 056001 (2016).
 - [9] L. D'Alessio, Y. Kafri, A. Polkovnikov, and M. Rigol, From Quantum Chaos and Eigenstate Thermalization to Statistical Mechanics and Thermodynamics, *Adv. Phys.* **65**, 239 (2016).
 - [10] F. Borgonovi, F. M. Izrailev, L. F. Santos, and V. G. Zelevinsky, Quantum chaos and thermalization in isolated

- systems of interacting particles, *Phys. Rep.* **626**, 1 (2016).
- [11] H. Tasaki, Typicality of Thermal Equilibrium and Thermalization in Isolated Macroscopic Quantum Systems, *J. Stat. Phys.* **163**, 937 (2016).
- [12] T. Langen, T. Gasenzer, and J. Schmiedmayer, Prethermalization and universal dynamics in near-integrable quantum systems, *J. Stat. Mech.* **064009** (2016).
- [13] R. Nandkishore and D. A. Huse, Many-body localization and thermalization in quantum statistical mechanics, *Annu. Rev. Condens. Matter Phys.* **6**, 15 (2015).
- [14] E. K. Sklyanin, Boundary conditions for integrable quantum systems, *J. Phys. A* **21**, 2375 (1988).
- [15] F. C. Alcaraz, M. N. Barber, M. T. Batchelor, R. J. Baxter, and G. R. W. Quispel, Surface exponents of the quantum XXZ, Ashkin-Teller and Potts models, *J. Phys. A* **20**, 6397 (1987).
- [16] N. Beisert, L. Fievet, M. de Leeuw, and F. Loebbert, Integrable deformations of the XXZ spin chain, *J. Stat. Mech.* **P09028** (2013).
- [17] See Supplemental Material at [URL will be inserted by publisher] for various analytical predictions regarding the quantities $\langle n|A^n\rangle$ and $\overline{C}_t(A)$, as well as for additional numerical results.
- [18] Numerically, we evaluated (3) by utilizing standard dynamical typicality and Runge-Kutta propagation methods, and (7) by diagonalization of H .
- [19] E. H. Lieb and D. W. Robinson, The finite group velocity of quantum spin systems, *Commun. Math. Phys.* **28**, 251 (1972).
- [20] J. Stolze, A. Nöppert, and G. Müller, Gaussian, exponential, and power-law decay of time-dependent correlation functions in quantum spin chains, *Phys. Rev. B* **52**, 4319 (1995).
- [21] S. Bravyi, M. B. Hastings, and F. Verstraete, Lieb-Robinson bounds and the generation of correlations and topological quantum order, *Phys. Rev. Lett.* **97**, 050401 (2006).
- [22] F. H. L. Essler and M. Fagotti, Quench dynamics and relaxation in isolated integrable quantum spin chains, *J. Stat. Mech.* **6**, 064002 (2016).
- [23] C. Duval and M. Kastner, Quantum kinetic perturbation theory for near-integrable spin chains with weak long-range interactions, *New J. Phys.* **21**, 093021 (2019).
- [24] J. Kemp, N. Y. Yao, C. R. Laumann, and P. Fendley, Long coherence times for edge spins, *J. Stat. Mech.* **063105** (2017).
- [25] A. M. Alhambra, J. Riddell, and L. P. Garcia-Pintos, Time evolution of correlation functions in quantum many-body systems, *Phys. Rev. Lett.* **124**, 110605 (2020).
- [26] P. Reimann, Foundation of statistical mechanics under experimentally realistic conditions, *Phys. Rev. Lett.* **101**, 190403 (2008); N. Linden, S. Popescu, A. J. Short, and A. Winter, Quantum mechanical evolution towards equilibrium, *Phys. Rev. E* **79**, 061103 (2009); A. J. Short, Equilibration of quantum systems and subsystems, *New J. Phys.* **13**, 053009 (2011); P. Reimann and M. Kastner, Equilibration of macroscopic quantum systems, *New J. Phys.* **14**, 043020 (2012); A. J. Short and T. C. Farrelly, Quantum equilibration in finite time, *New J. Phys.* **14**, 013063 (2012); B. N. Balz and P. Reimann, Equilibration of isolated many-body quantum systems with respect to general distinguishability measures, *Phys. Rev. E* **93**, 062107 (2016).
- [27] G. S. Uhrig, J. Hackmann, D. Stanek, J. Stolze, and F. B. Anders, Conservation laws protect dynamic spin correlations from decay: Limited role of integrability in the central spin model, *Phys. Rev. B* **90**, 060301(R) (2014).
- [28] H. Touchette, Equivalence and nonequivalence of ensembles: thermodynamic, macrostate, and measure levels, *J. Stat. Phys.* **159**, 987 (2015); F. G. S. L. Brandao and M. Cramer, Equivalence of Statistical Mechanical Ensembles for Non-Critical Quantum Systems, arXiv:1502.03263; H. Tasaki, On the local equivalence between the canonical and the microcanonical ensembles for quantum spin systems, *J. Stat. Phys.* **172**, 905 (2018); T. Kuwahara and K. Saito, Gaussian concentration bound and ensemble equivalence in generic quantum many-body systems including long-range interactions, *Ann. Phys.* **421**, 168278 (2020).
- [29] For a very large class of translationally invariant models it has been rigorously shown in Ref. [25] that $\overline{C}(A)$ must go to zero in the thermodynamic limit. The opposite behavior of $\overline{C}(A)$ in our present model and in the spin-chain and central spin models in Refs. [24, 27, 30–33] does not contradict Ref. [25] since translational invariance is violated in all these models.
- [30] J. Stolze, V. S. Viswanath, and G. Müller, Dynamics of semi-infinite quantum spin chains at $T = \infty$, *Z. Phys. B* **89**, 45 (1992).
- [31] J. Stolze and M. Vogel, Impurity spin relaxation in $S = 1/2$ XX chains, *Phys. Rev. B* **61**, 4026 (2000).
- [32] I. A. Maceira and F. Mila, Infinite coherence time of edge spins in finite-length chains, *Phys. Rev. B.* **97**, 064424 (2018).
- [33] S. Grijalva, J. De Nardis, and V. Terras, Open XXZ chain and boundary modes at zero temperature, *SciPost Phys.* **7**, 023 (2019).
- [34] Namely, setting $J_z = g = 0$ in (1) and $\beta = 0$ in (2), the long-time average $\overline{C}(\sigma_1^x)$ for $L \rightarrow \infty$ was found in Sec. 2.4 of Ref. [30] to be positive if $J_x > J_y > 0$ and zero if $J_y \geq J_x > 0$.
- [35] P. Fendley, Strong zero modes and eigenstate phase transitions in the XYZ/interacting Majorana chain, *J. Phys. A: Math. Theor.* **49**, 30LT01 (2016).
- [36] G. Niccoli and V. Terras, Correlation functions for open XXZ spin 1/2 quantum chains with unparallel boundary magnetic fields, *J. Phys. A: Math. Theor.* **55**, 405203 (2022).
- [37] G. Biroli, C. Kollath, and A. M. Läuchli, Effect of Rare Fluctuations on the Thermalization of Isolated Quantum Systems, *Phys. Rev. Lett.* **105**, 250401 (2010); V. Alba, Eigenstate thermalization hypothesis and integrability in quantum spin chains, *Phys. Rev. B* **91**, 155123 (2015); T. Mori, Weak eigenstate thermalization with large deviation bound, arXiv:1609.09776; E. Iyoda, K. Kaneko, and T. Sagawa, Fluctuation Theorem for Many-Body Pure Quantum States, *Phys. Rev. Lett.* **119**, 100601 (2017); T. Kuwahara and K. Saito, Eigenstate thermalization from the clustering property of correlations, *Phys. Rev. Lett.* **124**, 200604 (2020).
- [38] The cluster decomposition principle means that the spatial (equal-time) correlations of local operators vanish in the limit of large separations between them, see e.g. Refs. [7, 8] for recent reviews and Refs. [39, 40] for particularly early pertinent works.
- [39] E. H. Wichmann and J. H. Crichton, Cluster decomposition properties of the S matrix, *Phys. Rev.* **132**, 2788 (1963).
- [40] S. Weinberg, What is quantum field theory, and what did

we think it is?, arXiv:hep-th/9702027

- [41] Some reasons are: In our case, it is important that the system is at thermal equilibrium, exhibits many degrees of freedom, and that temporal (rather than spatial) correlations are considered. On the other hand, the fundamental subtleties of the quantum mechanical measurement process play no prominent role in our case.

SUPPLEMENTAL MATERIAL

Section I provides the derivation of various analytical predictions – mostly regarding the quantities $\langle n|A|n\rangle$ and $C_t(A)$ – which were stated throughout the main paper. Of particular interest will be single-spin observables of the form $A = s_l^a$, but also a large class of more general A will be covered.

Section II contains the additional numerical examples and remarks, as announced throughout the main paper.

I. ANALYTICAL PREDICTIONS

As in the main paper, we consider XYZ model Hamiltonians

$$H = g s_1^z - \sum_{l=1}^{L-1} J_x s_{l+1}^x s_l^x + J_y s_{l+1}^y s_l^y + J_z s_{l+1}^z s_l^z, \quad (\text{S1})$$

with an impurity at site $l = 1$ and spin-1/2 operators s_l^a , where $l \in \{1, \dots, L\}$ and $a \in \{x, y, z\}$. For the time being, the couplings g and J_a may still be arbitrary.

Denoting the eigenvalues and eigenvectors of H as E_n and $|n\rangle$ (with $n = 1, \dots, N := 2^L$), the thermal expectation value of an observable A ,

$$\langle A \rangle_{\text{th}} := \text{tr}\{A e^{-\beta H}\} / \text{tr}\{e^{-\beta H}\}, \quad (\text{S2})$$

can be rewritten as

$$\langle A \rangle_{\text{th}} = \sum_{n=1}^N p_n \langle n|A|n\rangle, \quad (\text{S3})$$

$$p_n := e^{-\beta E_n} / \sum_{m=1}^N e^{-\beta E_m}, \quad (\text{S4})$$

and its dynamic correlation function

$$\begin{aligned} C_t(A) &:= \langle AA(t) \rangle_{\text{th}} - \langle A \rangle_{\text{th}}^2 \\ &= \langle A e^{iHt} A e^{-iHt} \rangle_{\text{th}} - \langle A \rangle_{\text{th}}^2 \end{aligned} \quad (\text{S5})$$

(Heisenberg picture in units with $\hbar = 1$) as

$$C_t(A) := \sum_{m,n=1}^N p_n |\langle m|A|n\rangle|^2 e^{i(E_m - E_n)t} - \langle A \rangle_{\text{th}}^2. \quad (\text{S6})$$

One thus can conclude that the time-averaged correlations

$$\overline{C}(A) := \lim_{T \rightarrow \infty} \frac{1}{T} \int_0^T dt C_t(A) \quad (\text{S7})$$

can be rewritten in the form

$$\begin{aligned} \overline{C}(A) &= \sum_{n=1}^N p_n [\langle n|A|n\rangle]^2 - \left[\sum_{n=1}^N p_n \langle n|A|n\rangle \right]^2 \\ &= \sum_{n=1}^N p_n [\langle n|A|n\rangle - \langle A \rangle_{\text{th}}]^2, \end{aligned} \quad (\text{S8})$$

where, in case of degeneracies, the eigenstates $|n\rangle$ must be chosen so that A is diagonal in the corresponding eigenspaces of H . [This guarantees that $\langle m|A|n\rangle = 0$ for all $m \neq n$ with $E_m = E_n$ in (S6).]

A. Basic symmetries

Recalling that the operators $2s_l^a$ can be identified with Pauli matrices (in units with $\hbar = 1$), one readily verifies that those $2s_l^a$ are unitary and Hermitian operators, and that $s_l^x s_l^z = -s_l^z s_l^x$. It follows that also the so-called *spin-flip operator*

$$U_z := \prod_{l=1}^L 2s_l^z \quad (\text{S9})$$

is a unitary and Hermitian operator, satisfying $U_z = U_z^\dagger = U_z^{-1}$, and that

$$U_z s_l^x = -s_l^x U_z \quad (\text{S10})$$

for any given $l \in \{1, \dots, L\}$. Likewise, one finds that

$$U_z s_l^y = -s_l^y U_z, \quad (\text{S11})$$

$$U_z s_l^z = s_l^z U_z \quad (\text{S12})$$

for all $l \in \{1, \dots, L\}$.

Let us now assume that B is an arbitrary product of factors of the form s_l^a , where the indices a and l may or may not be different for each factor. Let us moreover assume that the number of factors with the property $a \in \{x, y\}$ is even. For instance, each term on the right-hand side of (S1) is of this form. It readily follows that $U_z B = B U_z$, and hence

$$U_z H = H U_z, \quad (\text{S13})$$

often referred to as *spin-flip* or Z_2 *symmetry* of H . Likewise, if the number of factors with the property $a \in \{x, y\}$ is odd, then $U_z B = -B U_z$. In particular,

$$U_z s_l^a = -s_l^a U_z \text{ for } a \in \{x, y\} \quad (\text{S14})$$

and any $l \in \{1, \dots, L\}$.

Since H and U_z commute (see (S13)), there exists a common set of eigenvectors $|n\rangle$, and since U_z is unitary, all its eigenvalues are of unit modulus, implying that $\langle n|U_z^\dagger A U_z|n\rangle = \langle n|A|n\rangle$ for any Hermitian operator A . On the other hand, for the specific operators $A = s_l^a$ with $a \in \{x, y\}$ we can conclude from (S14) that $\langle n|U_z^\dagger A U_z|n\rangle = -\langle n|A|n\rangle$. Altogether, we thus obtain

$$\langle n|s_l^a|n\rangle = 0 \text{ for } a \in \{x, y\} \quad (\text{S15})$$

and any $l \in \{1, \dots, L\}$.

Assuming that $g = 0$ in (S1), and generalizing the definition (S9) to

$$U_a := \prod_{l=1}^L 2s_l^a, \quad (\text{S16})$$

one finds, similarly as in (S13), that $U_a H = H U_a$ for any $a \in \{x, y, z\}$. Assuming furthermore that L is even, the operator U_x contains an even number of factors of the form s_l^x , hence it must commute with U_z (see above (S13)). Analogously, $U_a U_b = U_b U_a$ for all $a, b \in \{x, y, z\}$. Similarly as above Eq. (S15), one thus can conclude that there must exist a common set of eigenvectors $|n\rangle$ for H , U_x , U_y , and U_z with the property

$$\langle n | s_l^a | n \rangle = 0 \text{ for } a \in \{x, y, z\} \quad (\text{S17})$$

and any $l \in \{1, \dots, L\}$ provided L is even and $g = 0$.

B. Degenerate and non-degenerate Hamiltonians

If the Hamiltonian H in (S1) does not exhibit any degeneracies then its eigenvectors $|n\rangle$ are unique (up to irrelevant complex phases and permutations of n), hence the extra condition below (S8) is trivially fulfilled (for any Hermitian A). Focusing on such Hamiltonians H and on $A = s_l^a$ with $a \in \{x, y\}$, we thus can conclude that (S8) and (S15) apply simultaneously, implying

$$\overline{C}(s_l^a) = 0 \text{ for } a \in \{x, y\} \quad (\text{S18})$$

and any $l \in \{1, \dots, L\}$. Similarly, one concludes from (S8) and (S17) that

$$\overline{C}(s_l^a) = 0 \text{ for } a \in \{x, y, z\} \quad (\text{S19})$$

and any $l \in \{1, \dots, L\}$ provided L is even and $g = 0$.

On the other hand, if H exhibits at least one degeneracy, the extra condition below (S8) may in general be violated by the specific basis $|n\rangle$ appearing in (S15) and (S17). Hence, our present symmetry considerations do not admit any relevant conclusions with respect to the actual key quantity (S7) of the main paper. In particular, the relations (S18) and (S19) may possibly no longer apply, and are indeed numerically observed to be violated in general (see also Sec. II below).

Next we analytically demonstrate the existence of degeneracies in two important cases:

First, we consider *cases with odd L and $g = 0$* in (S1). As said above Eq. (S15), there exists a common set of eigenvectors $|n\rangle$ of H and U_z . The corresponding eigenvalues are denoted as E_n and λ_n , respectively. Since H and U_z are Hermitian, all E_n and λ_n must be real, and since U_z is unitary, all λ_n must be of unit modulus. Focusing on an arbitrary but fixed $|n\rangle$, let us define $|\tilde{n}\rangle := U_x |n\rangle$. Exploiting $U_x H = H U_x$ (see below Eq. (S16)), it readily follows that both $|n\rangle$ and $|\tilde{n}\rangle$ are

eigenvectors of H with the same eigenvalue E_n . On the other hand, since L is odd and $g = 0$, one finds similarly as above Eqs. (S13) and below (S16) that $U_x U_z = -U_z U_x$, implying that $U_z |\tilde{n}\rangle = -\lambda_n |\tilde{n}\rangle$. Recalling that $U_z |n\rangle = \lambda_n |n\rangle$ and that λ_n is of unit modulus it follows that $|n\rangle$ and $|\tilde{n}\rangle$ must be linearly independent. In conclusion, *for odd L and $g = 0$ all eigenvalues of H must be at least two-fold degenerate.*

Second, we again consider *cases with $g = 0$, but now, we moreover require that $J_x = J_y$* in (S1), i.e., we are dealing with the so-called XXZ model. It readily follows that the magnetization $S_z := \sum_{l=1}^L s_l^z$ commutes with H . Similarly as before, H and S_z thus exhibit a common set of eigenvectors $|n\rangle$ with corresponding (real) eigenvalues E_n and μ_n , respectively. Defining again $|\tilde{n}\rangle := U_x |n\rangle$ and exploiting $U_x H = H U_x$ (see below Eq. (S16)), both $|n\rangle$ and $|\tilde{n}\rangle$ must be eigenvectors of H with the same eigenvalue E_n . Similarly as in (S14), one furthermore finds that $s_l^z U_x = -U_x s_l^z$, implying $S_z U_x = -U_x S_z$ and thus $S_z |\tilde{n}\rangle = -\mu_n |\tilde{n}\rangle$. As before, we can conclude that *all eigenvalues of H must be at least twofold degenerate with the possible exception of those with $\mu_n = 0$* (corresponding to the so-called zero magnetization subsector, which only exists for even L).

For symmetry reasons, the same conclusions apply whenever $g = 0$ and the couplings $J_{x,y,z}$ are not pairwise different.

Generally speaking, the existence of degeneracies can often be rigorously deduced from certain symmetries, as exemplified above, or from some other *a priori* reasons. On the other hand, to rigorously prove the *non-existence* of degeneracies is usually very difficult or even impossible. In particular, the absence of any symmetry or other *a priori* reasons for degeneracies still does not exclude the existence of “accidental degeneracies” (which then are, however, often expected or observed to be structurally unstable and thus restricted to a set of model parameter values of measure zero). This very difficult task to analytically demonstrate the absence of degeneracies goes beyond the scope of our present work. On the other hand (and as said in the main paper), we numerically observed that our above conditions seem to be not only sufficient but (generically) also necessary for the occurrence of degeneracies (at least for all examples we actually examined).

On the basis of this numerical evidence we thus henceforth take it for granted that, generically, the relation (S18) applies whenever $g \neq 0$. Likewise, (S19) applies in all cases with $g = 0$, even L , and pairwise different $J_{x,y,z}$.

C. Further symmetry considerations

Incidentally, for $g = 0$ the Hamiltonian (S1) also satisfies the well-known, so-called parity or reflection symmetry [S1]. In the absence of degeneracies it follows that the eigenstates $|n\rangle$ must be at the same time eigenstates

of the parity operator. However, this insight is of limited value for our present purposes. [One only recovers the obvious fact that in the absence of the impurity ($g = 0$) all thermal equilibrium properties are invariant under $l \mapsto L + 1 - l$.] On the other hand, in the above mentioned cases where the occurrence of (at least two-fold) degeneracies can be shown analytically, the parity symmetry may give rise to more than two-fold degeneracies.

Next, we turn to a generalization of the basic symmetry considerations from Sec. IA. Similarly as above (S13), let us denote by A_a^+ an arbitrary product of factors of the form s_l^b , where the indices b and l may or may not be different for each factor, but such that the number of factors with the property $b \neq a$ is even. Moreover, the symbol A_a^+ may also represent an arbitrary linear combination of such operators. Finally, the symbol A^+ represents any linear combination of such operators A_a^+ with arbitrary $a \in \{x, y, z\}$. Likewise, the symbols A_a^- refers to odd instead of even numbers with the property $b \neq a$, and analogously for A^- . Similarly as in (S15) one then can conclude that

$$\langle n | A_z^- | n \rangle = 0 \quad (\text{S20})$$

for any such operator A_z^- . Under the same precondition as in (S18), which in turn applies whenever $g \neq 0$ (see end of previous subsection), it follows that

$$\overline{\mathcal{C}}(A_z^-) = 0. \quad (\text{S21})$$

In the same vein, for $g = 0$ and even L the generalization of (S17) takes the form

$$\langle n | A^- | n \rangle = 0 \quad (\text{S22})$$

for any A^- as specified above. Under the additional condition of pairwise different couplings $J_{x,y,z}$ one similarly can conclude that the generalization of (S19) takes the form

$$\overline{\mathcal{C}}(A^-) = 0 \quad (\text{S23})$$

for any A^- .

Note that any observable A can be rewritten in the form $A^+ + A^-$. The set of observables covered by (S22) and (S23) is thus already quite large.

D. Symmetries of thermal expectation values and correlation functions under a sign change of g

Let us consider Hamiltonians of the general structure

$$H = gH_x^- + H_x^+, \quad (\text{S24})$$

where H_x^\pm are of the form as specified above (S20). A particular example is our original model from (S1). Our main goal is a comparison of such a Hamiltonian (S24) and its counterpart

$$\tilde{H} := -gH_x^- + H_x^+. \quad (\text{S25})$$

In other words, we are interested in the consequences of a sign change of g in (S1), or, more generally, in (S24). Moreover, we will focus on observables A_x^\pm as specified above (S20). Particularly interesting examples of the type A_x^- are

$$A_x^- = s_l^z. \quad (\text{S26})$$

Similarly as above (S14), one readily verifies that

$$U_x A_x^\pm = \pm A_x^\pm U_x. \quad (\text{S27})$$

Together with (S24) and (S25) we thus obtain

$$\tilde{H} U_x = U_x H. \quad (\text{S28})$$

Recalling that $U_x = U_x^\dagger$ (since U_x is simultaneously unitary and Hermitian), it is thus natural to generally define

$$\tilde{A} := U_x A U_x \quad (\text{S29})$$

for any given operator A . Exploiting (S27) we can conclude that

$$\tilde{A}_x^\pm = \pm A_x^\pm. \quad (\text{S30})$$

As before, we denote by $|n\rangle$ and E_n the eigenvectors and eigenvalues of H , and we define

$$|\tilde{n}\rangle := U_x |n\rangle. \quad (\text{S31})$$

Exploiting (S28), one readily infers that $\tilde{H} |\tilde{n}\rangle = E_n |\tilde{n}\rangle$, i.e., the eigenvectors of \tilde{H} are related to those of H via (S31), and the corresponding eigenvalues are identical for \tilde{H} and H . Note that if H exhibits degeneracies, these conclusions apply to any choice of the basis $|n\rangle$.

Similarly as for the thermal expectation values of a system with Hamiltonian H in (S2), let us abbreviate those of a system with Hamiltonian \tilde{H} as

$$\langle A \rangle_{\tilde{\text{th}}} := \text{tr}\{A e^{-\beta \tilde{H}}\} / \text{tr}\{e^{-\beta \tilde{H}}\}. \quad (\text{S32})$$

Together with Eqs. (S3), (S4), and the discussion around (S31) we can conclude that

$$\langle A \rangle_{\tilde{\text{th}}} = \sum_{n=1}^N p_n \langle \tilde{n} | A | \tilde{n} \rangle. \quad (\text{S33})$$

Exploiting (S29) and (S31) we thus obtain

$$\langle A \rangle_{\tilde{\text{th}}} = \sum_{n=1}^N p_n \langle n | \tilde{A} | n \rangle. \quad (\text{S34})$$

Together with (S30) and (S3) we can conclude that

$$\langle A_x^\pm \rangle_{\tilde{\text{th}}} = \pm \langle A_x^\pm \rangle_{\text{th}}. \quad (\text{S35})$$

In other words, upon switching the sign of g in (S1) (or more generally in (S24)), thermal expectation values of observables of the type A_x^\pm remain unchanged, while

thermal expectation values of observables of the type A_x^- simply change their sign. Particular examples of the latter type are the spin operators s_l^z in (S26). Further examples will be provided in Eq. (S38) below.

In the same vein, the correlation functions (S5) can be rewritten in the form (S6) for a system with Hamiltonian H , and (by similar arguments as in the derivation of (S34)) as

$$\tilde{C}_t(A) := \sum_{m,n=1}^N p_n |\langle m | \tilde{A} | n \rangle|^2 e^{i(E_m - E_n)t} - \langle A \rangle_{\text{th}}^2 \quad (\text{S36})$$

for a system with Hamiltonian \tilde{H} . Again by means of almost the same steps as before, this finally yields the result

$$\tilde{C}_t(A_x^\pm) = C_t(A_x^\pm). \quad (\text{S37})$$

In other words, we arrive at our main result that correlation functions of arbitrary observables of the type A_x^\pm are invariant under a sign change of g in (S1) (or, more generally, in (S24)). The same invariance is inherited by the time-averaged correlation functions (S7).

Note that any observable A of the form

$$A = \prod_{k=1}^K s_{l_k}^{a_k} \quad (\text{S38})$$

with arbitrary $a_k \in \{x, y, z\}$, $l_k \in \{1, \dots, L\}$, and $K \in \mathbb{N}$ is either of the form A_x^+ or of the form A_x^- . For any such observable A , the correlation functions $C_t(A)$ are thus invariant under a sign change of g , while the thermal expectation values are either invariant or inverted (see below (S35)).

Analogous conclusions as in (S35) and (S37) are readily recovered also for observables of the type A_y^\pm .

E. Symmetries under sign changes of two J_a

Let us define, similarly as in (S16), for any given $a \in \{x, y, z\}$ the even-site spin-flip operator

$$U_a^e := \prod_{\text{even } l} 2s_l^a, \quad (\text{S39})$$

where the product runs over all even $l \in \{1, \dots, L\}$. Similarly as in Sec. IA, one can conclude that

$$U_a^e s_l^a = s_l^a U_a^e \quad (\text{S40})$$

for all $l \in \{1, \dots, L\}$ and $a \in \{x, y, z\}$. It follows that

$$U_a^e s_l^a s_{l+1}^a = s_l^a s_{l+1}^a U_a^e \quad (\text{S41})$$

for all $l \in \{1, \dots, L-1\}$ and $a \in \{x, y, z\}$. Analogously, one finds for arbitrary $a, b \in \{x, y, z\}$ with $a \neq b$ that

$$U_a^e s_l^b = -s_l^b U_a^e \text{ for even } l \in \{1, \dots, L\}, \quad (\text{S42})$$

$$U_a^e s_l^b = s_l^b U_a^e \text{ for odd } l \in \{1, \dots, L\}, \quad (\text{S43})$$

$$U_a^e s_l^b s_{l+1}^b = -s_l^b s_{l+1}^b U_a^e \text{ for all } l \in \{1, \dots, L-1\}. \quad (\text{S44})$$

Generalizations to other observables (cf. previous subsections) and to odd-site spin-flip operators are straightforward but not essential in the following.

Denoting by $H(g, J_x, J_y, J_z)$ the Hamiltonian (S1) for an arbitrary but fixed set of parameters g, J_x, J_y, J_z , and exploiting the various above derived relations, it follows that

$$U_x^e H(g, J_x, J_y, J_z) = H(g, J_x, -J_y, -J_z) U_x^e, \quad (\text{S45})$$

$$U_y^e H(g, J_x, J_y, J_z) = H(g, -J_x, J_y, -J_z) U_y^e, \quad (\text{S46})$$

$$U_z^e H(g, J_x, J_y, J_z) = H(g, -J_x, -J_y, J_z) U_z^e. \quad (\text{S47})$$

Returning to the abbreviation $H := H(g, J_x, J_y, J_z)$, denoting by $|n\rangle$ and E_n the eigenvectors and eigenvalues of H , and defining

$$|\tilde{n}\rangle := U_x^e |n\rangle, \quad (\text{S48})$$

$$\tilde{H} := H(g, J_x, -J_y, -J_z), \quad (\text{S49})$$

we thus can infer from (S45) that $\tilde{H}|\tilde{n}\rangle = E_n|\tilde{n}\rangle$, i.e., the eigenvectors of \tilde{H} are related to those of H via (S48), and the corresponding eigenvalues are identical for \tilde{H} and H . Moreover, by exploiting (S40) and (S42), one can conclude that

$$\langle \tilde{n} | s_l^a | \tilde{n} \rangle = \pm \langle n | s_l^a | n \rangle, \quad (\text{S50})$$

where the minus sign applies if l is even and $a \neq x$, and the plus sign otherwise.

By almost the same line of reasoning as in the previous subsection one now can conclude that the thermal expectation values for $A = s_l^a$ in (S2)-(S4) are the same for H and \tilde{H} if the plus sign applies in (S50), and of opposite sign otherwise. According to (S49), this is tantamount to a simultaneous sign change of J_y and J_z . Likewise, the correlation functions for $A = s_z^a$ in (S5)-(S7) are found to be invariant under a simultaneous sign change of J_y and J_z .

By exploiting the symmetry (S46) or (S47) instead of (S45), analogous conclusions are found to apply for a simultaneous sign change of J_x and J_z , or of J_x and J_y , respectively.

F. Symmetries under a sign changes of one J_a

According to (S1) and (S2), thermal expectation values of arbitrary observables A are left invariant when simultaneously changing the sign of all five model parameters β, g, J_x, J_y, J_z . Likewise, one can infer from (S5) that dynamical correlation functions exhibit a complex conjugation under a simultaneous sign change of β, g, J_x, J_y, J_z , while their long-time average in (S7) is left invariant (note that the right-hand side of (S8) is purely real).

Focusing on observables of the form $A = s_l^a$, dynamical correlation functions were found to be invariant under a sign change of g in Sec. ID, and under a simultaneous

sign change of two among the three parameters J_x, J_y, J_z in Sec. IE.

Upon properly combining all these various possibilities to change the sign of certain parameters, we thus can conclude that changing the sign of β and of one among the three parameters J_x, J_y, J_z results in a complex conjugation of the dynamical correlation functions and leaves their long-time average invariant, at least for all observables of the form $A = s_l^a$.

The corresponding transformation behavior when simultaneously changing the sign of two or three of the parameters J_x, J_y, J_z follows by sequentially carrying out one sign change after the other.

Analogous conclusions can be obtained for the thermal expectation values of s_l^a , but they are of no immediate relevance in the main paper.

The overall main result of the last three subsections is that one can focus on non-negative J_a and g , as it is done

in the main paper and in the subsequent section.

II. ADDITIONAL NUMERICAL EXAMPLES

Hereafter, our supplemental numerical results are presented in the order they are announced in the main paper. Also some additional observations and remarks are included in the accompanying text.

Fig.S1 provides further numerical evidence for the large- L asymptotics as detailed in the main paper at the end of the discussion of Fig.3 therein. As an interesting side remark we observe that all the slopes (decay rates) in Fig.S1 (d) are (nearly) equal, while the offsets (pre-exponential constants) increase upon approaching the chain's ends. This provides some additional insight how the large- L asymptotics when keeping l/L fixed matches the asymptotics when keeping l (or $L-l$) fixed.

Fig. S2 was announced in the discussion of Fig. 4 in the main paper, plotting once more the same data as in Fig. 5 of the main paper, but now on a semi-logarithmic scale. Some further interesting features of Fig.4 in the main paper will be addressed in the context of Fig.S6 below.

The remaining Figs. S3-S7 illustrate the items (a)-(c) in the first paragraph of Sec. IV in the main paper.

Specifically, the case of odd system sizes L in item (a) is exemplified by Fig. S3. Likewise, Fig. S4 illustrates item (a) for a case, where the couplings $J_{x,y,z}$ are not

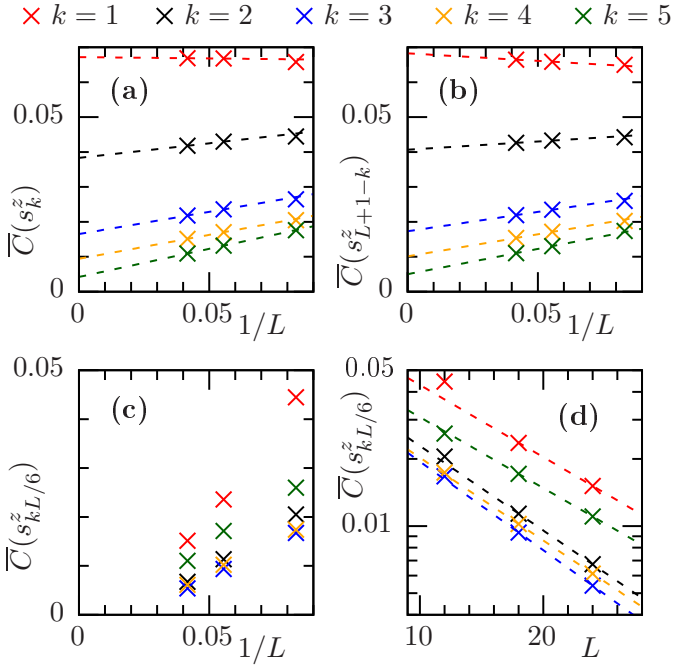


FIG. S1. Same as in Fig. 3 of the main paper, but now for a larger variety of different l -values. In more detail: Long-time averages $\overline{C}(s_l^z)$ by numerically evaluating (S7) for large but finite T are depicted for the XYZ model from (S1) with $g = 0.1$, $J_x = 1$, $J_y = 1.2$, $J_z = 1.5$, and $L \in \{12, 18, 24\}$, employing $\beta = 0.2$ in (S2)-(S5). (a) Results for $l = k \in \{1, 2, \dots, 5\}$, corresponding to the 5 leftmost sites of the chain. (b) Results for $l = L + 1 - k \in \{L - 4, L - 3, \dots, L\}$, corresponding to the 5 rightmost sites of the chain. (c) Results for $l = kL/6 \in \{L/6, 2L/6, \dots, 5L/6\}$, corresponding to 5 sites in the “bulk” of the chain. [These l -values are the reason for our focusing on $L \in \{12, 18, 24\}$.] (d) Same data as in (c), but now plotted semi-logarithmically versus L . The dotted lines are a guide to the eye, suggesting the convergence towards a positive large- L limit in (a) and (b), and an exponential decay towards zero in (d).

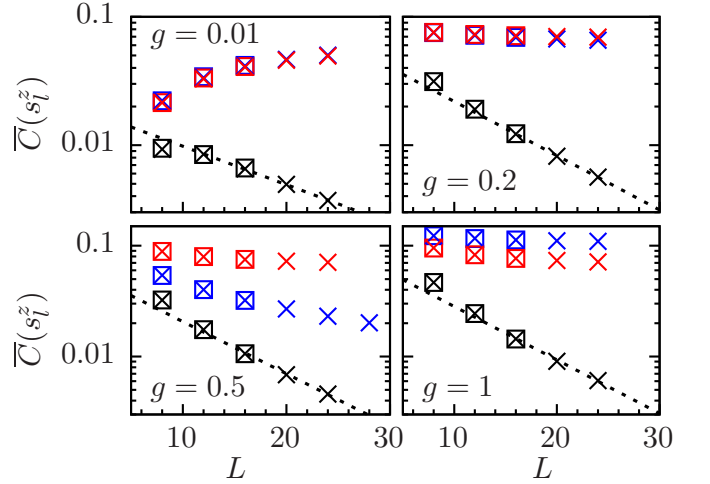


FIG. S2. Same data as in Fig.5 of the main paper, but now plotted semi-logarithmically versus L . In more detail: Long-time averages $\overline{C}(s_l^z)$ from (S7) are plotted versus L for the XYZ model from (S1) with $J_x = 1$, $J_y = 1.2$, $J_z = 1.5$, and different g -values (see legends), employing $\beta = 0.2$ in (S2)-(S5). Blue, black, and red symbols refer to $l = 1$, $l = L/2$, and $l = L$, respectively. Crosses: Numerical results by evaluating (S7) for large but finite T . Squares: Numerically exact (but also more expensive) results by evaluating (S8) via diagonalization of H . The dotted lines are a guide to the eye, suggesting an exponentially decaying large- L asymptotics of the black symbols.

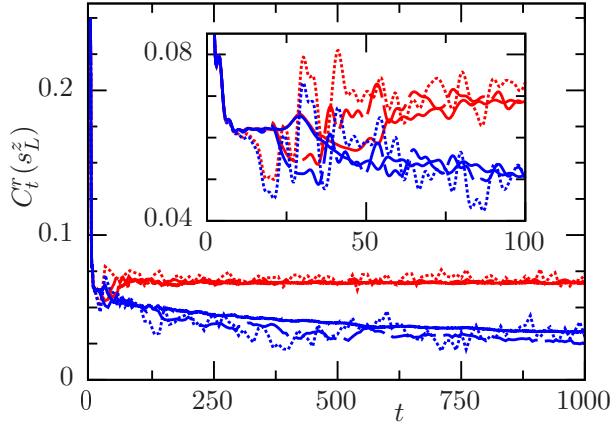


FIG. S3. Same as in Fig. 1 of the main paper, but now for odd instead of even system sizes L , namely $L = 19$ (solid), $L = 13$ (dashed) and $L = 9$ (dotted).

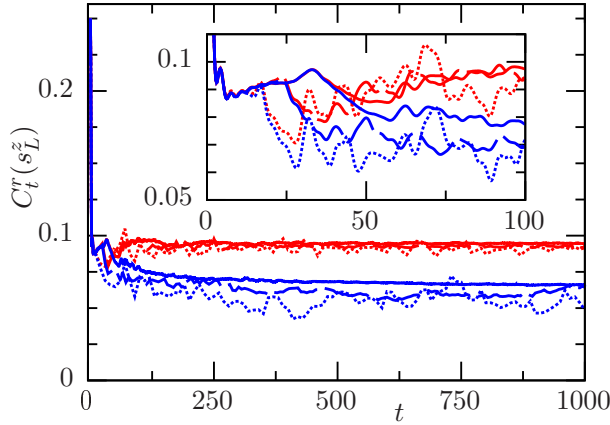


FIG. S4. Same as in as in Fig. 1 of the main paper, but now for couplings $J_{x,y,z}$ which are not pairwise different, namely $J_x = J_y = 1$, $J_z = 1.5$.

pairwise different (while L is again even). Essentially, the findings in both Fig. S3 and Fig. S4 are qualitatively quite similar to the case of even L and pairwise different $J_{x,y,z}$ (see Fig. 1 in the main paper), except that the blue curves no longer approach zero for large times t (see also Fig. S5 below). In other words, our analytical prediction $\overline{C}(s_i^z) = 0$ for $g = 0$ from (S19) is no longer applicable since (as detailed in Sec. IB) the Hamiltonian is known to exhibit degeneracies if L is odd or the $J_{x,y,z}$ are not pairwise different.

Accordingly, if L is odd or the $J_{x,y,z}$ are not pairwise different, the quantitative value of $\overline{C}(s_i^z)$ for $g = 0$, henceforth abbreviated as $\overline{C}_0(s_i^z)$, must be numerically determined. Fig. S5 exemplifies the finite-size scaling behavior of the long-time averages $\overline{C}(s_i^z)$ (for $g = 0.1$) and $\overline{C}_0(s_i^z)$ (for $g = 0$) in such a case where the $J_{x,y,z}$ are not pairwise different.

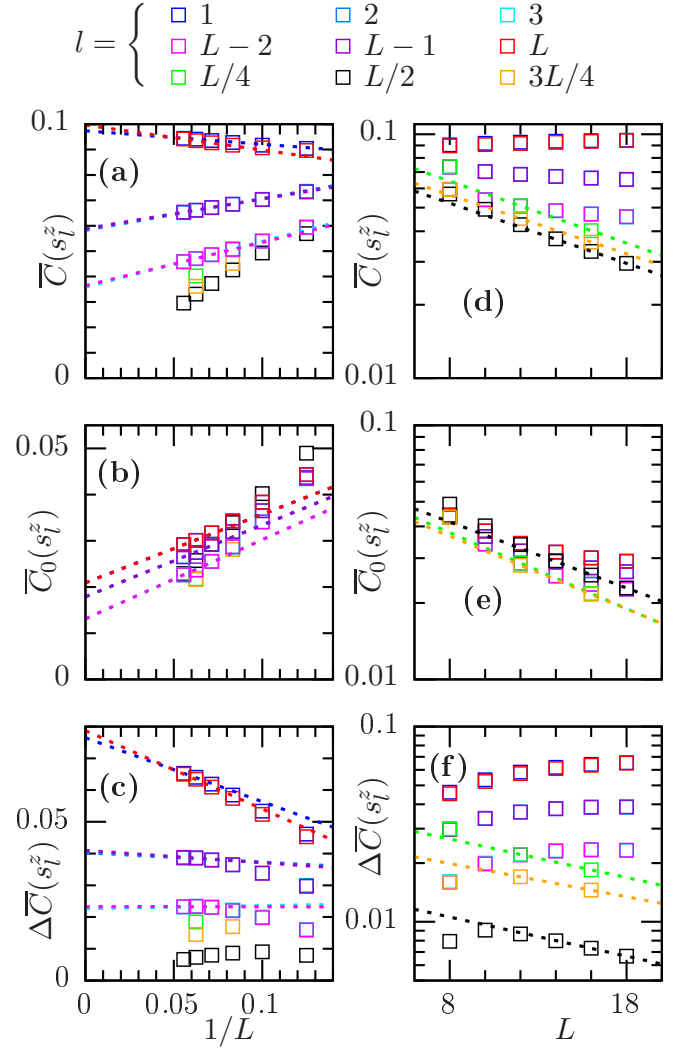


FIG. S5. (a): Long-time average $\overline{C}(s_i^z)$ by evaluating (S8) via numerically exact diagonalization of H versus $1/L$ for various l -values (see legend), employing the same system as in Fig. S4 ($g = 0.1$ and $J_{x,y,z}$ not pairwise different). (b) Same, but without impurity ($g = 0$), and denoting the long-time average as $\overline{C}_0(s_i^z)$. (c) Difference $\Delta\overline{C}(s_i^z) := \overline{C}(s_i^z) - \overline{C}_0(s_i^z)$ between the long-time averages in (a) and (b). (d)-(f): Same data as in (a)-(c) but now plotted semi-logarithmically versus L . Some symbols are (nearly) covered by others, and for $L \in \{10, 14\}$ there are no green and orange symbols. The dotted lines are a guide to the eye, suggesting the convergence towards a finite large- L limit in (a)-(c), and an exponential decay towards zero in (d)-(f).

In view of the quite slowly decaying blue curves in Fig. S4, the time-averaged correlations in Fig. S5 were *not* obtained by numerically evaluating (S7) for large but finite T , but rather by the numerically exact but also more expensive method to diagonalize H and then evaluate (S8). For this reason, the maximally achievable L -values in Fig. S5 are smaller than in our previous figures of this type.

Also shown in Fig. S5 is the quantity $\Delta\overline{C}(s_i^z) :=$

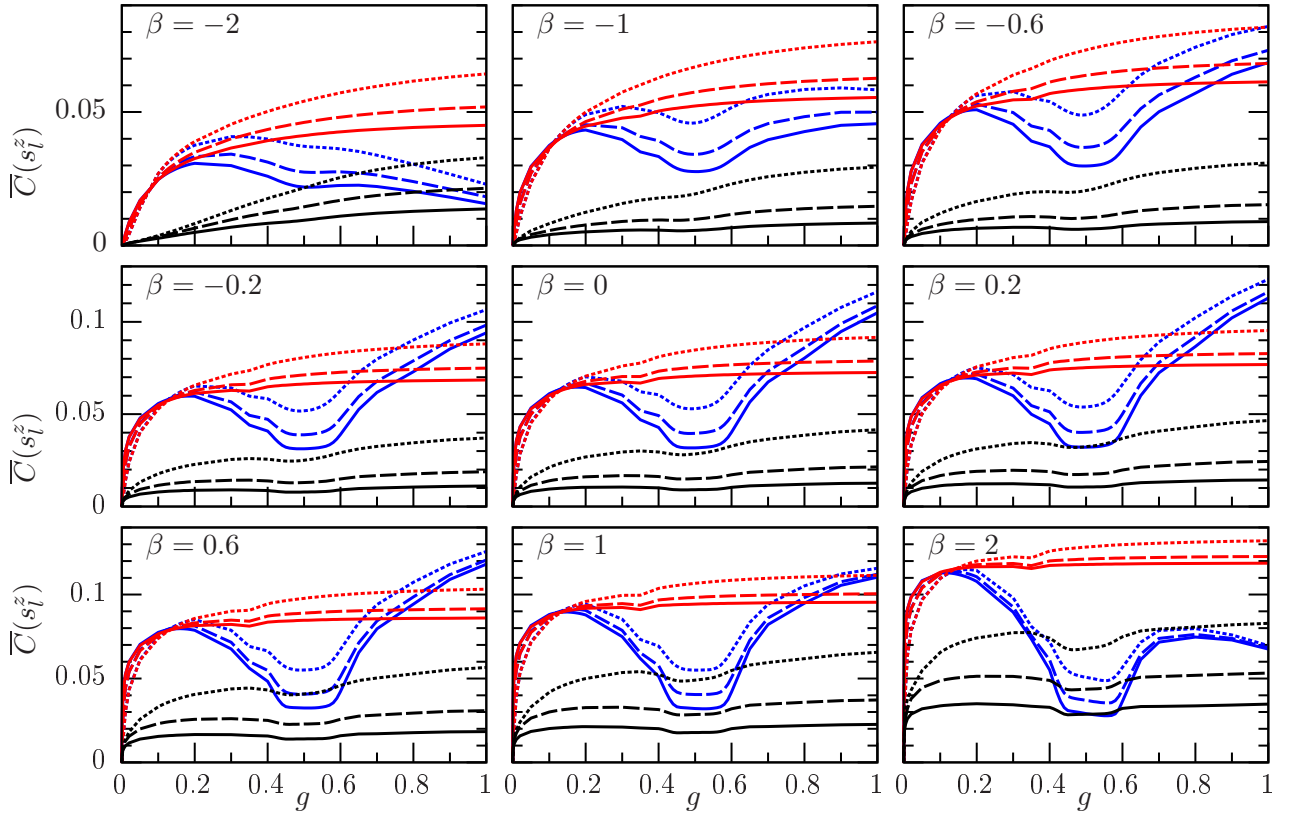


FIG. S6. Same as in Fig. 4 of the main paper, but now for various other values of β (see legend).

$\bar{C}(s_l^z) - \bar{C}_0(s_l^z)$. As already pointed out in the main paper, this quantity captures the characteristic signatures of allostery in such a case where our “usual” analytical prediction $\bar{C}_0(s_l^z) = 0$ no longer applies. In other words, Figs. S5 (c) and (d) essentially amount to the counterparts of Figs. 3(a) and (b) in the main paper, respectively, and indeed exhibit the same qualitative behavior.

Fig. S6 serves as a numerical illustration of item (b) in the main paper, namely the dependence of our findings on the parameter β in (S2)-(S8). Note that the spectrum of the Hamiltonian (S1) is bounded for any finite L , hence all the quantities in (S2)-(S8) are perfectly well-defined for arbitrary $\beta \in \mathbb{R}$. We also recall that the behavior for negative β is of particular interest with respect to the symmetry properties under a sign change of one (or three) of the couplings J_a (see Sec. IF). We finally remark that β represents the inverse temperature (in units with Boltzmann constant $k_B = 1$), and that the physical relevance and meaning of negative temperatures are sometimes still considered as not satisfactorily settled issues. This ongoing debate is only of very little relevance with respect to our actual main issues and therefore not further pursued.

Overall, the basic qualitative features in Fig. S6 change remarkably little upon variation of β . Without going into the details we mention that much stronger finite L -effects than in Fig. S6 are expected and observed to arise for

even much larger (positive) β -values (low temperatures), caused by two nearly degenerate lowest energy eigenvalues, which are separated by a gap from the rest of the spectrum.

Intuitively, one generally expects that the spin s_l^z at the site of the impurity ($l = 1$) will be forced for asymptotically large g to align with the impurity in (S1) and hence the correlations in (S5) will approach zero. On the other hand, the correlations away from the impurity site ($l > 1$) are not expected to approach zero but rather to approach some non-trivial (positive) large- g limit. Moreover, these effects are expected to require increasingly large g -values upon reducing the value of β in (S2)-(S8) (and may possibly even disappear for $\beta = 0$). Along these lines, one also may understand why the blue curves start to decrease in Fig. S6 for $\beta = \pm 2$ as g approaches unity, but not the red and black curves, and not for the smaller values of $|\beta|$ in Fig. S6.

On the basis of these considerations it also appears intuitively quite evident that a non-monotonic dependence of $\bar{C}(s_l^z)$ on g is, generally speaking, nothing unexpected, and likewise for the possibility that $\bar{C}(s_l^z)$ may assume smaller values at the location of the impurity ($l = 1$) than at the opposite chain end ($l = L$). The appearance of the extra (local) minima in Fig. S6 is harder to explain by simple arguments, but it seems not unlikely that somewhat similar basic mechanisms may be at work.

Finally, Fig. S7 exemplifies item (c) in the main paper, namely the disappearance of our allosteric impurity effects when J_z is no longer the largest among all three (positive) couplings $J_{x,y,z}$ (regarding negative couplings see Sec. IF). The salient point in Fig. S7 is that the correlations $\overline{C}(s_l^z)$ now indeed asymptotically approach zero for large L at both ends as well as in the middle of the chain. Whether $\overline{C}(s_l^z)$ decays exponentially with L , or as $1/L$ (or even in some other way) apparently still depends on l and on the choice of the couplings $J_{x,y,z}$. Moreover, the (approximate) equality of $\overline{C}(s_l^z)$ and $\overline{C}(s_{L+1-l}^z)$ (for sufficiently small g), which we observed in all previous examples, seems to be violated in the left plot in Fig. S7. A more detailed exploration of these issues will be presented elsewhere.

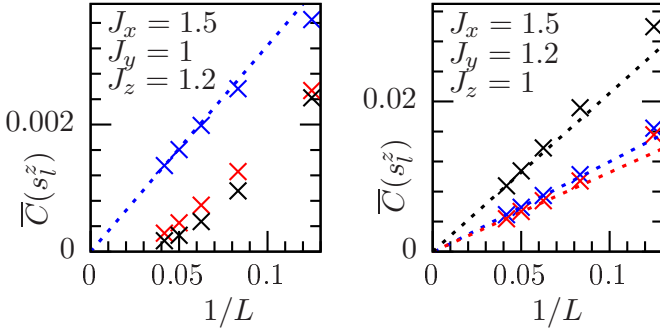


FIG. S7. Same as in Fig. 5 of the main paper, but now for other values of the couplings $J_{x,y,z}$ (see legends), and for $g = 0.1$ (see also Fig. S1, Fig. S2, and Fig. 3 in the main paper). In particular, the crosses once again represent time-averaged correlations $\overline{C}(s_l^z)$ for $l = 1$ (blue), $l = L$ (red) and $l = L/2$ (black).

[S1] K. Joel, D. Kollmar, and L. F. Santos, An introduction to the spectrum, symmetries, and dynamics of spin-1/2 Heisenberg chains, *Am. J. Phys.* **81**, 450 (2013).